A&A 657, A33 (2022)
https://doi.org/10.1051/0004-6361/202141750

Astronomy & Astrophysics

Lithium on the lower red giant branch of five Galactic globular clusters⋆,⋆⋆

C. Aguilera-Gómez[1,2], L. Monaco[1], A. Mucciarelli[3,4], M. Salaris[5], S. Villanova[6], and E. Pancino[7]

[1] Departamento de Ciencias Fisicas, Universidad Andres Bello, Fernandez Concha 700, Las Condes, Santiago, Chile
e-mail: craguile@uc.cl
[2] Núcleo de Astronomía, Universidad Diego Portales, Ejército 441, Santiago, Chile
[3] Dipartimento di Fisica e Astronomia, Universita degli Studi di Bologna, Via Gobetti 93/2, 40129 Bologna, Italy
[4] INAF – Osservatorio di Astrofisica e Scienza dello Spazio di Bologna, Via Gobetti 93/3, 40129 Bologna, Italy
[5] Astrophysics Research Institute, Liverpool John Moores University, IC2, Liverpool Science Park, 146 Brownlow Hill, Liverpool L3 5RF, UK
[6] Departamento de Astronomía, Universidad de Concepción, Casilla 160-C, Concepción, Chile
[7] INAF – Osservatorio Astrofisico di Arcetri, Largo Enrico Fermi 5, 50125 Firenze, Italy

Received 9 July 2021 / Accepted 22 September 2021

ABSTRACT

Context. Lithium is one of the few elements produced during Big Bang nucleosynthesis in the early universe. Moreover, its fragility makes it useful as a proxy for stellar environmental conditions. As such, the lithium abundance in old systems is at the core of various astrophysical investigations.
Aims. Stars on the lower red giant branch are key to studies of globular clusters where main sequence stars are too faint to be observed. We use these stars to analyze the initial Li content of the clusters and compare it to cosmological predictions, to measure spreads in Li between different stellar populations, and to study signs of extra depletion in these giants.
Methods. We used the GIRAFFE spectra to measure the lithium and sodium abundances of lower red giant branch stars in five globular clusters. These cover an extensive range in metallicity, from [Fe/H] ∼ −0.7 to [Fe/H] ∼ −2.3 dex.
Results. We find that the lithium abundance in these lower red giant branch stars forms a plateau, with values from $A(\mathrm{Li})_{\mathrm{NLTE}} = 0.84$ to 1.03 dex, showing no clear correlation with metallicity. When using stellar evolutionary models to calculate the primordial abundance of these clusters, we recover values of $A(\mathrm{Li})_{\mathrm{NLTE}} = 2.1-2.3$ dex, consistent with the constant value observed in warm metal-poor halo stars, namely the Spite plateau. Additionally, we find no difference in the lithium abundance of first and second population stars in each cluster. We also report the discovery of a Li-rich giant in the cluster NGC 3201, with $A(\mathrm{Li})_{\mathrm{NLTE}} = 1.63 \pm 0.18$ dex, where the enrichment mechanism is probably pollution from external sources.

Key words. globular clusters: general – stars: abundances – primordial nucleosynthesis – stars: chemically peculiar

1. Introduction

Lithium (Li) is one of the few elements that were produced minutes after the Big Bang during the Big Bang nucleosynthesis phase (BBN, Coc et al. 2014). Predictions of the production of elements in this theory are dependent solely on the baryon-to-photon ratio, a number that has been measured from the cosmic microwave background by WMAP (Hinshaw et al. 2013) and Planck (Planck Collaboration XVI 2014). Thus, the predicted amount of lithium formed in the early universe is $A(\mathrm{Li})$[1] = 2.69 ± 0.03 (Coc et al. 2014). The primitive lithium abundance, to be compared with predictions from the BBN, has been measured in old, metal-poor halo stars. This value is expected to be indicative of the primordial abundance, since stars that are this metal-poor do not have enough time at formation to be enriched with material from the interstellar medium or galactic sources producing Li (e.g., Prantzos 2012). Spite & Spite (1982a,b) found that halo dwarf stars with [Fe/H] between −2.4 and −1.4 dex and effective temperatures between 5700 and 6300 K share a similar abundance of $A(\mathrm{Li}) = 2.2$ dex, the so-called "Spite plateau", a result that has been confirmed in the halo (e.g., Charbonnel & Primas 2005; Meléndez et al. 2010) and in other environments such as globular clusters (e.g., Bonifacio 2002). The discrepancy between the predicted $A(\mathrm{Li})$ from the BBN and the measurements, over three times lower, is referred to as the "cosmic lithium problem". We note that Lithium is the only measured element produced during BBN that experiences such a discrepancy (Coc et al. 2014).

Moreover, to further complicate this picture, there is a decrease in the mean Li abundance and an increase in scatter at the lower-end metallicity of the Spite plateau, for metallicities [Fe/H] < −2.8, known as the "meltdown" (Sbordone et al. 2010, and references therein). However, very metal-poor stars have been found with higher Li abundances closer to the plateau (e.g., Bonifacio et al. 2018; Aguado et al. 2019).

Solutions for the discrepancy between Li measurements and predictions from BBN range from modifications to the BBN theory to processes affecting the stellar interiors and changing the Li abundance in old stars (see Fields 2011, for a review).

Lithium is an element often used as an indicator of chemical processes affecting the interior of stars, such as mixing, since it

⋆ Full Table A.1 is only available at the CDS via anonymous ftp to cdsarc.u-strasbg.fr (130.79.128.5) or via http://cdsarc.u-strasbg.fr/viz-bin/cat/J/A+A/657/A33
⋆⋆ Based on observations collected at the European Southern Observatory under ESO programme 095.D–0735(A).
[1] $A(\mathrm{Li}) = \log(n_{\mathrm{Li}}/n_{\mathrm{H}}) + 12$.

burns at temperatures (2.5×10^6 K) and densities found in main sequence stars. Thus, it is possible that a process such as diffusion (Fu et al. 2015) or additional turbulent mixing (Richard et al. 2005) is depleting the abundance in the stellar atmospheres of old stars which would not be indicative of BBN lithium.

Metal-poor globular clusters are among the oldest objects in the Galaxy (e.g., De Angeli et al. 2005). As such, their lithium is expected to closely resemble the abundance produced during BBN, making these systems important probes and tools in the study of the cosmic lithium problem. However, the measurement of Li abundance requires high-quality spectra, which are not easily obtained for the majority of cluster main sequence stars that are too faint. Thus, the Li abundance is known for dwarfs only for a handful of galactic clusters: M4 (Mucciarelli et al. 2011; Monaco et al. 2012), NGC 6397 (Lind et al. 2009b; González Hernández et al. 2009), NGC 7099 (Gruyters et al. 2016), NGC 6752 (Pasquini et al. 2005; Shen et al. 2010), 47 Tuc (D'Orazi et al. 2010; Dobrovolskas et al. 2014), Omega Centauri (Monaco et al. 2010), and M92 (Bonifacio 2002). In most of these clusters, the Li measured closely resembles that of the Spite Plateau, with the exception of 47 Tuc.

Additionally, globular clusters, once thought to be defined chemically by a single population of stars, with no dispersion in chemical abundances are now known to harbor populations with different light element abundances (Bastian & Lardo 2018). The second population of stars, which (according to current scenarios) would be born of the processed material from the first population, exhibiting high [Na/Fe] and low [O/Fe] that produces the observed sodium-oxygen anticorrelation in globular clusters (Carretta et al. 2009b,c). Given that the thermonuclear reactions that produce this pattern occur at higher temperatures than that required to burn Li, it is expected that a second population of stars should have a lower Li than the first population. However, only two clusters, with Li measured in their main sequence, show a hint of a Li-O correlation, 47 Tuc (Dobrovolskas et al. 2014), with no Li-Na anticorrelation, and NGC 6752 (Shen et al. 2010). In M4, there is a weak but statistically significant Li-Na anti-correlation (Monaco et al. 2012), while other clusters are shown to have similar Li in first and second population stars. The lack of a Li anticorrelation could be produced if the polluter of the second population has a significant Li production or if the material from the polluter is mixed with unprocessed material that preserved its initial lithium. Thus, studying the Li in globular clusters can aid in understanding their formation.

The lack of more numerous Li measurements in main sequence stars of globular clusters (due to their faintness) encourages the use of a complementary method, proposed by Mucciarelli et al. (2012), which uses lower red giant branch stars (LRGB). Red giant stars undergo a series of structural changes that produce alterations to their surface chemical abundances. The first of these processes is the first dredge-up (FDU), where the surface convective envelope of the stars deepens in mass, mixing material from the surface with the chemically processed interior. This translates into a decrease in the carbon and lithium abundances and an increase in the nitrogen abundance.

Standard stellar evolutionary models predict no other surface abundance changes on the red giant branch (RGB) after the end of the FDU. However, observations provide evidence of modified Li, C, N, O abundances as well as a modified C isotopic ratio after the RGB bump (Gratton et al. 2000). At this moment in stellar evolution, the advancing hydrogen-burning shell encounters and erases the discontinuity left in the chemical profile of the star by the deepest penetration of the convective envelope (Denissenkov & VandenBerg 2003), allowing extra-mixing to proceed (or do so more efficiently, e.g., Chanamé et al. 2005), bringing material from the stellar interior to the surface. The details of how this mechanism works and how it affects the stellar interiors are, however, not well understood.

Specifically, LRGBs are located between the end of the first dredge-up and the luminosity function bump. The dilution of lithium during the FDU at the beginning of the red giant phase is mass- and metallicity-dependent, but it is well characterized by stellar evolutionary models. This is why a complementary way of studying Li in old stars is to measure its abundance in LRGBs, where the A(Li) is constant at a given metallicity, mirroring the Spite plateau but at a lower value of $A(\mathrm{Li}) \sim 0.9-1.0$ dex that considers its depletion in the FDU. Moreover, the FDU mitigates the effects of diffusion, one of the main uncertainties for the interpretation of the Li abundance in dwarfs (Mucciarelli et al. 2011).

Mucciarelli et al. (2014) used this technique to study the primordial Li abundance of the globular cluster M54 located in the Sagittarius dwarf Spheroidal galaxy, providing evidence that the primordial Li is the same there as in the Milky Way and thus, that the cosmic lithium problem is Universal and not local. More evidence for this can be found in ω Cen, usually considered to be the remnant core of an accreted galaxy (e.g., Lee et al. 1999; Pancino et al. 2000), which also shows a consistent Li abundance with the Spite plateau (Monaco et al. 2010). The discovery of Gaia-Enceladus, a disrupted dwarf galaxy that was once accreted by the Milky Way and is now forming part of the galactic halo, allows for a new way to study the primordial Li content outside our Galaxy, confirming once again, the universality of the cosmic Li problem (Molaro et al. 2020; Simpson et al. 2021).

Confirming that the LRGB stars can also be used to study the formation of globular clusters, Mucciarelli et al. (2018) measure Li in LRGB stars of ω Cen, finding an extended Na-Li anticorrelation. However, this distribution seems to be rather complex, with the most metal-rich stars in the cluster always showing low Li abundances, but the metal-poor stars in the cluster can either show low sodium and normal Li, or high sodium with normal or depleted Li abundances.

Thus, as demonstrated by these works, the study of LRGBs allows for the characterization of the Li abundance pattern of clusters and the primordial Li in systems where dwarfs are too faint. Following this complementary approach, in this work we study the Li abundance of lower red giant branch stars of five Galactic globular clusters, providing new insights into the dependence of the RGB Li plateau on metallicity and its application in calculating the primordial Li abundance in these systems. A similar study of Li on RGB stars belonging to the Galactic globular cluster NGC 104 has recently been performed by Aoki et al. (2021).

Moreover, one of these clusters, NGC 6838 is a metal-rich globular cluster. The low Li abundance of dwarfs in the relatively metal-rich cluster 47 Tuc ([Fe/H] = −0.8 dex and $A(\mathrm{Li}) = 1.4$–2.2 dex, Dobrovolskas et al. 2014) when compared to the Spite plateau suggest that there is a depletion mechanism acting in the main sequence at higher metallicities, which is not found at lower metallicities, given that M4, with [Fe/H] = −1.1 dex shows Li consistent with the Spite plateau (Monaco et al. 2012). The study of NGC 6838 will allow us to test whether this is a peculiar pattern for 47 Tuc or if all metal-rich globular clusters are Li depleted. We also notice that NGC 3201 is significantly younger (∼2 Gyr) than the rest of the studied clusters (Marín-Franch et al. 2009).

In Sect. 2, we report the observations and evaluate membership of our targets to the globular clusters. We provide measurements of the atmospheric parameters in Sect. 3 as well as the lithium and sodium abundances (Sect. 4) of these stars. We report our results on the LRGB Li plateau, on the lack of a Li-Na correlation in these clusters, and on the discovery of a new Li-rich giant in NGC 3201 in Sect. 5. We present our summary in Sect. 6.

2. Observations and membership

We selected five clusters in the aim to cover the entire metallicity range of Halo globular clusters and to observe a large number of stars. We end up with NGC 4590 (M 68), NGC 6809 (M 55), NGC 6656 (M 22), NGC 3201, and NGC 6838 (M 71). For each of these five clusters, we selected our targets in the LRGB phase. The spectroscopic observations correspond to the ESO program 095.D–0735 (PI. A. Mucciarelli) and were carried out using the FLAMES multi-object spectrograph (Pasquini et al. 2002) at the Very Large Telescope (VLT). The GIRAFFE fibers provide mid-resolution spectra with $R \sim 18\,000$. The observations were performed in the setups HR15N, sampling the lithium resonance doublet at $\lambda \sim 6708$ Å, and HR12, sampling the sodium D doublet at $\lambda \sim 5890$–5896 Å for GIRAFFE.

A total of five exposures of 45 minutes each for NGC 6838, NGC 6809, NGC 6656, and NGC 3201, along with ten exposures for NGC 4590 were taken in the HR15N setup. Only one exposure for each star was needed in the HR12 setup, as the large equivalent width of the Na doublet requires smaller signal-to-noise ratios (S/N) to be measured.

The spectra were bias-subtracted, flat-fielded and wavelength-calibrated using the standard ESO pipelines[2]. In each exposure, some fibers were dedicated to measure spectra of the sky. These were median-combined to create a master sky, then subtracted to each of our science spectra.

Radial velocities for each individual spectra in the HR15N setup are measured using the IRAF[3] task *fxcor*. This task uses the cross correlation method, where we use as template a synthetic spectrum from Coelho et al. (2005), typical of a metal-poor red giant, with a resolution reduced so as to be similar to our spectra. The typical radial velocity precision is $\sim$2–3 km s^{-1} for each HR15N spectra of each star. This value is the formal fxcor error, related to the fitted function used to calculate the velocity (Tonry & Davis 1979). After shifting every spectrum to their rest-frame, we median-combine all spectra that correspond to a particular target to obtain an individual spectrum for each star that is later used in the analysis. By combining all the exposures we obtain an additional error in the radial velocity, corresponding to the standard deviation of different measurements for the same target. These are typically from $\sim$0.6–2.2 km s^{-1}. Signal-to-noise ratios per pixel (S/N) in the HR15N setup are typically around $\sim$70–300, while the single exposure for the HR12 allows us to obtain spectra with $S/N \sim 20$–70. Given the lower S/N of these spectra and the fewer number of lines clearly visible, we did not measure a radial velocity from this setup, but instead we assumed the average radial velocity measured from the HR15N spectra. After obtaining a unique radial velocity for each target star, we used these values to construct radial velocity distributions in each cluster. These were fitted with a Gaussian profile, where a mean and a standard deviation are calculated and used as criteria for membership.

[2] http://www.eso.org/sci/software/pipelines/

[3] IRAF is distributed by the National Optical Astronomy Observatories, which are operated by the Association of Universities for Research in Astronomy, Inc., under cooperative agreement with the National Science Foundation.

Table 1. Mean radial velocity (RV) for each cluster.

Cluster	Mean RV (km s^{-1})	SD (km s^{-1})	Harris RV (km s^{-1})	Harris SD (km s^{-1})
NGC 4590	−94.2	3.2	−94.7	2.5
NGC 6809	174.9	4.6	174.7	4.0
NGC 6656	−146.5	7.8	−146.3	7.8
NGC 3201	495.0	3.8	494.0	5.0
NGC 6838	−22.9	3.5	−22.8	2.3

Notes. Mean radial velocity (RV) for each cluster and standard deviation (SD) of each radial velocity distribution and comparisons with Harris (1996, 2010 edition).

2.1. Cluster membership

For each cluster, we excluded stars with radial velocities that were significantly different with respect to the mean radial velocity of the sample stars (a difference higher than 3σ). Additionally, we used the membership probability reported for each star in these clusters by Vasiliev & Baumgardt (2021) which makes use of the Early Data Release 3 (EDR3) for the *Gaia* mission (Gaia Collaboration 2018), considering that stars are members if they have a membership probability $P_{\rm mem} > 0.9$.

The cluster NGC 6838 is in a particularly contaminated field. With a Gaussian distribution, we get the mean radial velocity of the cluster and remove all the stars outside 2σ as field contaminants. Only 35 out of the 117 observed stars are within that radial velocity range and have astrometric parameters consistent with the cluster.

In NGC 6809, from the originally observed 110 stars, 95 remain after excluding stars by their membership probability or radial velocity. In NGC 6656, 101 of the 112 observed stars are consistent with being cluster members. In NGC 4590, we kept 50 of 69 observed stars, and in NGC 3201, 98 out of the 117 observed stars are consistent with the cluster membership.

All of our measured mean radial velocities are reported in Table 1 and are consistent with those in the catalog from Harris (1996, 2010 edition).

3. Atmospheric parameters

Effective temperatures for stars are derived photometrically, using the (*V–I*) color and the Alonso et al. (1999) relations. For all of our clusters, we use the photometry of Stetson et al. (2019) and transform to Johnson (*V–I*) colors using the relation in Bessell (1983).

To calculate dereddened colors, we use extinction coefficients from McCall (2004). The adopted color excess $E(B–V)$ and distance modulus for each cluster can be found in Table 2. While the color excess of NGC 6838 is high, it does not suffer from significant differential reddening ($\langle \delta E(B–V) \rangle$ = 0.035 mag, Bonatto et al. 2013). For the clusters NGC 6656 and NGC 3201, we corrected for differential reddening using the maps of Alonso-García et al. (2012) with zero-point $E(B–V) = 0.33$ (Schlegel et al. 1998) for NGC 6656, as suggested by that work and of Pancino et al. (in prep.), with zero-point $E(B–V) = 0.24$ for NGC 3201 (Bonatto et al. 2013).

Table 2. Color excess *E(B–V)* and distance modulus for each cluster.

Cluster	*E(B–V)*	Source [(a)]	$(m-M)_0$	Source [(b)]
–	–	–	mag	–
NGC 4590	0.06	SF11	15.00	K+15
NGC 6809	0.12	SF11	13.95	VBD18
NGC 6656*	0.33	S+98	13.60	H10
NGC 3201*	0.24	B+13	14.20	H10
NGC 6838	0.28	SF11	13.80	H10

Notes. Adopted color excess *E(B–V)* and distance modulus adopted for each cluster. Clusters marked with * were corrected by differential reddening.
References. [(a)]SF11: Schlafly & Finkbeiner (2011); S+98: Schlegel et al. (1998); B+13: Bonatto et al. (2013). [(b)]VBD18: VandenBerg & Denissenkov (2018); K+15: Kains et al. (2015); H10: Harris (1996, 2010 edition).

Table 3. Mean metallicity and number of members for each cluster.

Cluster	[Fe/H]	$SD_{[Fe/H]}$	Harris [Fe/H]	Members
–	dex	dex	dex	–
NGC 4590	−2.34	0.10	−2.23	46
NGC 6809	−1.79	0.10	−1.94	90
NGC 6656	−1.77	0.12	−1.70	98
NGC 3201	−1.58	0.06	−1.59	83
NGC 6838	−0.72	0.07	−0.78	32

Notes. Mean metallicity, standard deviation (SD), and number of members for each cluster. Metallicity values reported by Harris (1996, 2010 edition) are also included.

The surface gravity was calculated for each star using isochrone fitting and a set of MIST isochrones (Dotter 2016; Choi et al. 2016) restricting ages to be higher than 12 Gyr. In particular, we placed the star in an effective temperature-absolute magnitude plane and compare its position there with the theoretical isochrones, using the estimated metallicity of the cluster from Harris (1996, 2010 edition) to prevent degeneracy. We built a probability distribution with all the isochrone points in a 3σ radius from the input parameters. This method was preferred to measuring $\log g$ spectroscopically given the lack of a relevant number of Fe II lines in our spectra. Additionally, Mucciarelli & Bonifacio (2020) recommend to use photometric temperatures and gravities in low-metallicity stars of globular clusters, since spectroscopic parameters are lower than photometric determinations and inconsistent with the position of the giants in color-magnitude diagrams.

We compared the calculated $\log g$ with $\log g$ estimated using bolometric luminosity of the giants and we find a good agreement between both methods. The uncertainties obtained are $\Delta \log g \simeq 0.2$ dex. As for the error in effective temperature, we adopted typical uncertainties of $\Delta T_{\rm eff} \simeq 125$ K, which correspond to the standard deviation of the color relation used (Alonso et al. 1999).

Microturbulence velocities are then calculated for each star using their effective temperature, $\log g$, and the relation in Bruntt et al. (2012). The typical errors when using this relation are reported to be 0.13 km s^{-1} by the authors. However, this value depends on uncertainties in effective temperature and $\log g$, assumed to be 100 K and 0.1 dex, respectively. Given that our uncertainties are slightly higher, we assume a typical error in microturbulence velocity of 0.15 km s^{-1}.

We calculated metallicities for each star individually by measuring the equivalent width of Fe I lines using the code DAOSPEC (Stetson & Pancino 2008) through the wrapper 4DAO[4] (Mucciarelli 2013). Then, the Fe abundances were derived with the code GALA (Mucciarelli et al. 2013). Our Fe I line list was constructed by using the spectra of the coldest and hottest giants in the sample. We visually inspected the spectra to identify lines that were visible in both stars covering the entire effective temperature range. Although we initially considered a large list of lines, a spurious correlation between metallicity and effective temperature was identified in some of the clusters, with an extremely strong correlation in NGC 3201. We only selected lines that did not saturate in any cluster and, as such, were shown to be good indicators of the real metallicity of the star. Based on this test, we ended up selecting six lines with a linear correlation between equivalent widths and temperatures to only estimate the metallicity, and used it as an additional criteria of membership. We then calculated the mean metallicity of the sample and adopted that value for all stars of the cluster when we determine chemical abundances. We estimated the NLTE corrections for our selected Fe I lines, that could be relevant for metal-poor stars (Bergemann et al. 2012). Only two of the used lines have NLTE corrections reported by Mashonkina et al. (2016); in the temperature and $\log g$ ranges of NGC 4590 stars, they amount to ∼0.072−0.085 dex. These are the maximum values expected for our sample of stars, because NLTE corrections are larger for lower metallicities. We find no way to apply consistently Fe NLTE corrections, but these seem to be smaller than the reported uncertainty in metallicity, and would not affect significantly the measured abundances.

Table 3 shows the mean metallicity and final number of members in each cluster. In NGC 3201, we found some outliers in the metallicity distribution, which are likely non members, and were removed with sigma-clipping, using a criteria of 2σ. We aim for the maximum purity of the sample rather than completeness and, thus, although we might exclude some members, this procedure increases the probability of membership by selecting stars with metallicities closer to the mean of the cluster. We note that while the mean metallicity of NGC 3201 is similar in different literature sources, there is an ongoing debate about the existence of an intrinsic metallicity spread in the cluster (Albornoz et al. 2021, and references therein). Given that we are selecting only stars with a metallicity similar to the mean of the cluster, the conclusion about the possible spread in the metallicity distribution should not change our results. The mean metallicity value we obtain for NGC 6809 is [Fe/H] = −1.79 ± 0.10. The metallicity of this cluster seems to be controversial, with some measurements similar to the value we report here (e.g., Kayser et al. 2008), and others closer to the [Fe/H] = −1.94 value found in the Harris catalog (e.g., Carretta et al. 2009a). The final parameters for member stars in each of the five clusters can be found in Table A.1, fully available at the CDS.

4. Chemical abundances

4.1. Lithium

Lithium abundances are calculated using spectral synthesis around the Li doublet at wavelength ∼6708 Å. The observed spectrum was compared to synthetic spectra generated using MOOG (Sneden 1973, 2018 version), with ATLAS9 model

[4] http://www.cosmic-lab.eu/4dao/4dao.php

atmospheres (Castelli & Kurucz 2003) and the abundance derived through χ^2 minimization. The continuum level, one of the greatest uncertainties in the determination of Li abundance with this method, was set by using a region of ∼10 Å, around the Li line. For some of the giants where the Li line is not detected, only upper limits are reported. We estimated the detection limits on Li using the relation by Cayrel (1988) for the minimum equivalent width that could be measured in each spectra, and calculate the corresponding lithium abundance for three times that limiting equivalent width.

We calculated non-local thermodynamical equilibrium (NLTE) corrections using the grid of Lind et al. (2009a). In NGC 3201, NGC 4590, and NGC 6656, the corrections are usually smaller than 0.1 dex; whereas in NGC 6809, the corrections are even smaller (<0.06 dex). In contrast, NGC 6838 has greater corrections, from 0.01 dex to 0.15 dex. Two stars in NGC 4590 are outside the limits of the grid, and thus we use the closest grid point as the values for the Li correction.

The error in lithium was calculated by adding in quadrature the uncertainties associated with the synthetic spectra producing the best fit, which greatly depends on the positioning of the continuum and the propagation of errors in stellar parameters, in particular, of effective temperature, which produces the greatest deviations in A(Li). The typical uncertainties due to the quality of the data are of the order of $\Delta A(\mathrm{Li}) \sim 0.05$ dex, which depends on the S/N of the spectrum. This refers to uncertainties in the fitting procedure, including continuum placement and adjustments in the fit due to small changes in the radial velocity and line broadening. NGC 3201 is the cluster with the overall worst quality spectra and, as such, it can show higher errors of up to $\Delta A(\mathrm{Li}) \sim 0.08$ dex. Uncertainties in the Li abundance arising from the propagation of errors in the stellar parameters are 0.10−0.17 dex due to $T_{\rm eff}$, 0.00−0.02 dex due to the metallicity, and 0.01−0.03 dex because of errors in $\log g$. Errors propagated from the microturbulence velocity (of ∼0.01 dex) are added linearly, given that microturbulence velocity depends on effective temperature and $\log g$. Our typical uncertainties are $\Delta A(\mathrm{Li}) \simeq 0.16$ dex.

As a sanity check, we calculated the Li abundance in the cluster M4 using the same spectra used in Mucciarelli et al. (2011). The A(Li) we calculated using the same parameters as reported in that work is very similar for the RGB stars. We calculated an average difference of $\langle \delta A(\mathrm{Li}) \rangle = 0.09$. No attempt was made to reproduce the measurements in turn-off stars, as those are out of the scope of this paper. To check that our parameter determination was also consistent with previous literature, we also re-calculated stellar parameters from photometry directly, finding similar values and A(Li), with an average difference of $\langle \delta A(\mathrm{Li}) \rangle = 0.16$.

4.2. Sodium

The sodium abundance was measured from the Na D doublet at 5890−5896 Å, also using spectral synthesis of the region and thus generating a grid of synthetic spectra using SPECTRUM (Gray & Corbally 1994), with the same ATLAS9 model atmosphere. The choice of using one code over another was only done based on the convenience of our available wrappers and methods. However, we tested to see the difference between abundances using the two radiative transfer codes. Abundances of sodium change at most by 0.05 dex over the range of parameters of our sample. The best fit was selected with χ^2 minimization. The continuum placing is complicated by the low S/N of some of our spectra in the region. Accordingly, the errors in Na abundance consider these uncertainties. Uncertainties due to the continuum placement and quality of the fit can be as high as 0.10 dex. The propagation of errors in the stellar parameters gives typical Na uncertainties of ∼0.11 dex due to $T_{\rm eff}$, ∼0.14 dex because of errors in $\log g$, as well as ∼0.01 dex uncertainty due to metallicity and ∼0.02 dex due to uncertainties in the microturbulence velocity. Typical uncertainties then are $\Delta A(\mathrm{Na}) \simeq 0.18$ dex.

We applied the Na NLTE corrections computed by Lind et al. (2011), that can be substantial for sodium measured from the D doublet, even reaching values of −0.5 dex within our sample. It was not possible to measure sodium in NGC 6838 due to the presence of contamination by interstellar sodium in that region of the spectra, close to the position of the stellar Na lines.

Typical spectra from our sample in the regions of the Li line and Na doublet is shown in Fig. 1. These spectra show the quality of our data and typical fits to the Li and Na lines to measure abundances. In the right panels, we also see the strong interstellar sodium lines.

5. Results

The NLTE lithium and sodium abundances of the LRGB stars in the studied globular clusters are found in Table A.1, available online. We also include LTE abundances in the online data. We show our measured Li abundances as a function of V magnitude and the position of member stars in their color magnitude diagrams in Figs. 2 and 3 (left and right panels, respectively). The magnitudes are also corrected by differential reddening in these figures. Lithium upper limits are shown as blue arrows. The position of the luminosity function bump (Samus et al. 1995; Ferraro et al. 1999) is indicated for each cluster as a dashed line, and the background corresponds to the catalog from Stetson et al. (2019), cleaned using membership probabilities by Vasiliev & Baumgardt (2021), but without corrections by differential reddening. Lithium upper limits in all five clusters are above our reported measurements and, as such, are consistent with the abundances reported.

We first notice here that some of the stars show unusual positions in the color-magnitude diagram. This is because our initial selection of targets was not done using the Stetson photometry. We study each of these stars independently and follow them throughout our analysis to make sure they are not contaminating our sample and confusing our results.

In NGC 4590, the star ID35003 is not located in the locus of RGB stars of the cluster. This star has a proper motion, radial velocity, and metallicity consistent with NGC 4590. We also check an independent measurement of its $\log g$ using bolometric corrections and find a very similar value between both determinations. However, given its color, this star has a higher temperature and higher lithium abundance (A(Li) = 0.81 dex) than other stars in the RGB of that magnitude. This star can be clearly identified in the left panel of Fig. 2 with higher Li abundance. Thus, although this result is consistent given our analysis, we consider that this star may not be part of the cluster due to its unusual position in the color-magnitude diagram. Thus, we removed it from further analysis.

NGC 6656 shows a broad RGB even after corrections by differential reddening. The bluer sequence does not show a particular spatial location, indicating that this is probably not the effect of additional differential reddening and that the broad sequence might be due to the spatial resolution of the used reddening maps. This cluster is suspected to have an intrinsic iron spread (Da Costa et al. 2009), but also see Mucciarelli et al. (2015).

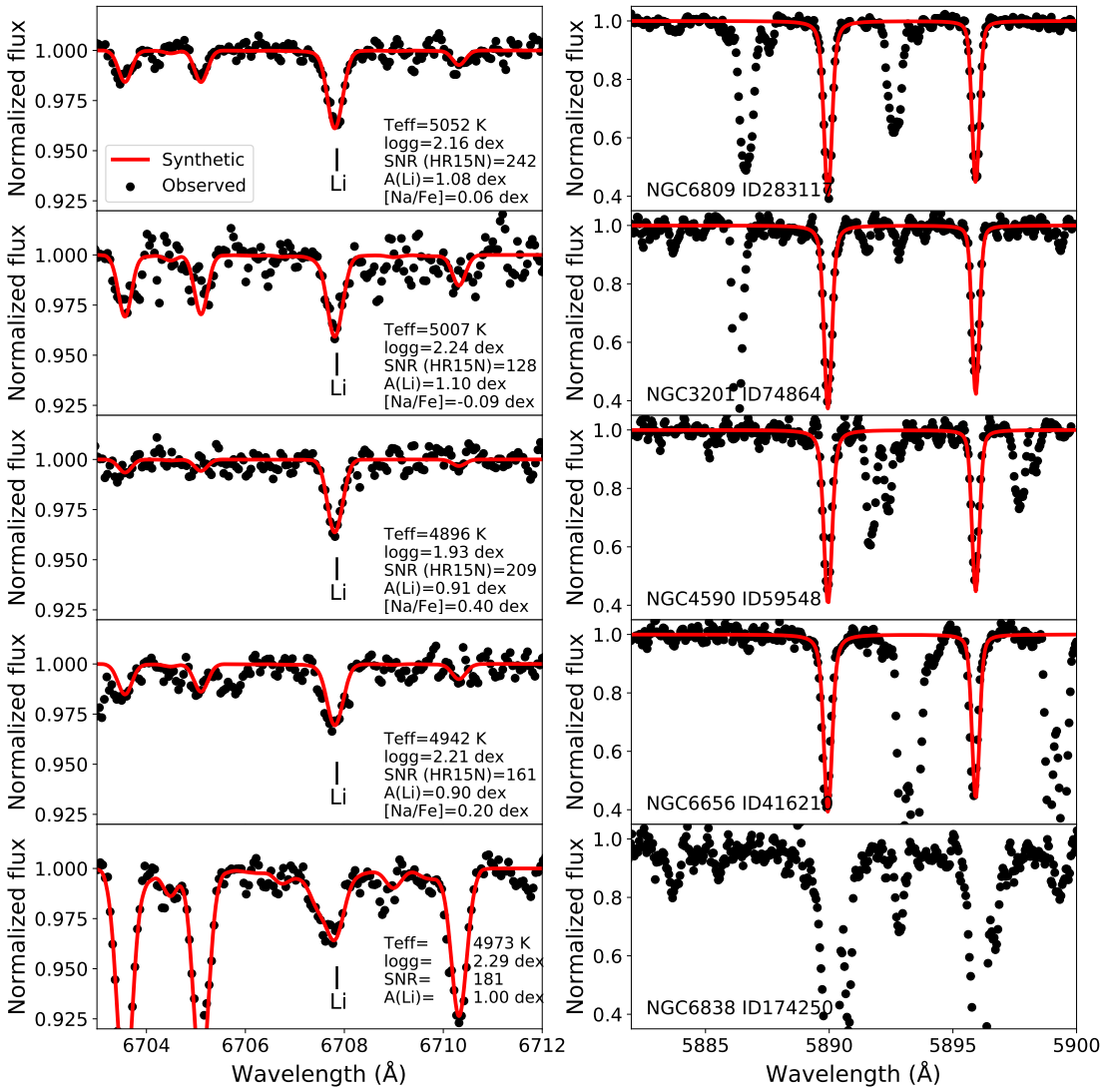

Fig. 1. Spectra from one typical sample star in each of the clusters in the region of the Li line (*left*) and the Na doublet (*right*), and the respective synthetic fits to the lines to measure the abundances. Stellar parameters, NLTE abundances, and S/N of the spectra are indicated for each star.

In some of the clusters, we can identify the position of the end of the FDU and the RGB bump in both panels, with abrupt decreases in A(Li). In NGC 4590, we can clearly identify stars going through the FDU, diluting their Li at $V \sim 17$ mag, then a plateau formed by the LRGB and a second decrease in A(Li) produced by the inclusion of giants located after the luminosity function bump. Most of the upper RGB stars have only Li upper limits. Cluster NGC 6809 has two stars after the RGB bump, while NGC 3201 has only one, that shows a smaller Li abundance than the rest of RGB stars, at the level of the lower envelope of the Li distribution of LRGBs. We are able to identify the end of the FDU in NGC 3201, where stars at the bottom of the RGB decrease their Li abundances. The Li dilution due to FDU in NGC 6656 or NGC 6838 is not clearly visible. In NGC 6656, the abundance slowly decreases as we move up in the giant branch, with a large scatter and the plateau is not as clear as in other clusters.

We also notice that there is a giant in NGC 3201 (namely giant ID 97812, a red star symbol in Fig. 3) with unusually high Li abundance $A(\mathrm{Li})_{\mathrm{NLTE}} = 1.63 \pm 0.18$ dex. Given that it is located before the onset of efficient extra-mixing, this Li-rich giant has probably experienced pollution from an external source. We analyze it further in Sect. 5.3.

5.1. LRGB plateau and the cosmic Li problem

To better identify a possible LRGB plateau in the five globular clusters, we binned the Li abundance as a function of effective temperature in Figs. 4 and 5. Left panel shows the Li abundance as a function of effective temperature, where we include upper limits as blue arrows. The right panel shows the binned abundance as blue points but only considering Li measurements (gray points) and no upper limits. To select stars that belong to the plateau, we defined the end of the first dredge-up by using the measured Li abundances. We performed a simple bilinear fit to the data in the A(Li)-T_{eff} diagram, from the highest temperature to the luminosity function bump, which is clearly signposted by the sharp drop of Li abundances with decreasing temperature. The fit provides the approximate temperature where the abundance plateau starts, whilst the luminosity function bump marks its end. We note that in NGC 4590 there are no stars that have completed the first dredge-up, as suggested by our fit to the data.

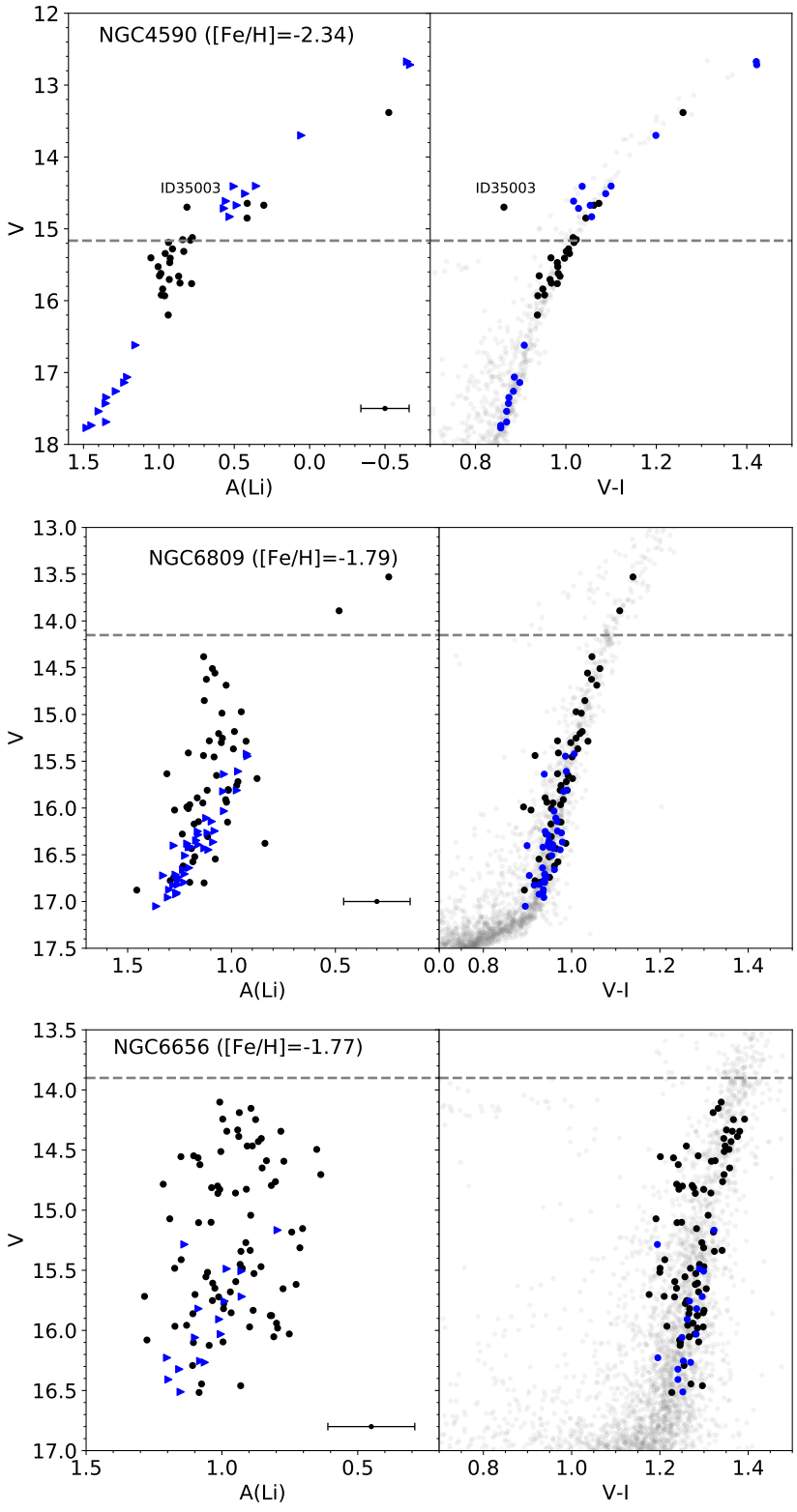

Fig. 2. Lithium abundances of NGC 4590 (*top panels*), NGC 6809 (*middle panels*), and NGC 6656 (*bottom panels*) as a function of V magnitude (*left panels*) alongside their respective color-magnitude diagrams (*right panels*). Blue symbols are Li upper limits. The approximate position of the luminosity function bump in each cluster is marked with a dashed line.

We identify the bins that belong to the LRGB plateau as red squares, which are the values we use to calculate the mean Li abundance of the plateau in each cluster. The stars are binned in equal-sized temperature ranges within each cluster to make sure that there is a significant number of stars in each bin; changing the bin size does not significantly alter our results.

The binned Li abundance allows us to better identify the LRGB plateau present in the clusters. In NGC 4590, the value of this plateau is $A(\mathrm{Li}) = 0.90 \pm 0.08$ dex. The error reported here is the standard deviation of the individual abundances of stars at the plateau. NGC 6809 shows a clear decrease in Li at the start of the RGB until reaching a plateau of $A(\mathrm{Li}) = 1.03 \pm 0.08$ dex. The effects of the FDU can also be observed in NGC 6656, where in this case, the LRGB reach a value of $A(\mathrm{Li}) = 0.88 \pm 0.09$ dex. In NGC 6838, we also identify a mean Li in LRGB stars of $A(\mathrm{Li}) = 0.84 \pm 0.10$ dex. The only cluster where the LRGB do

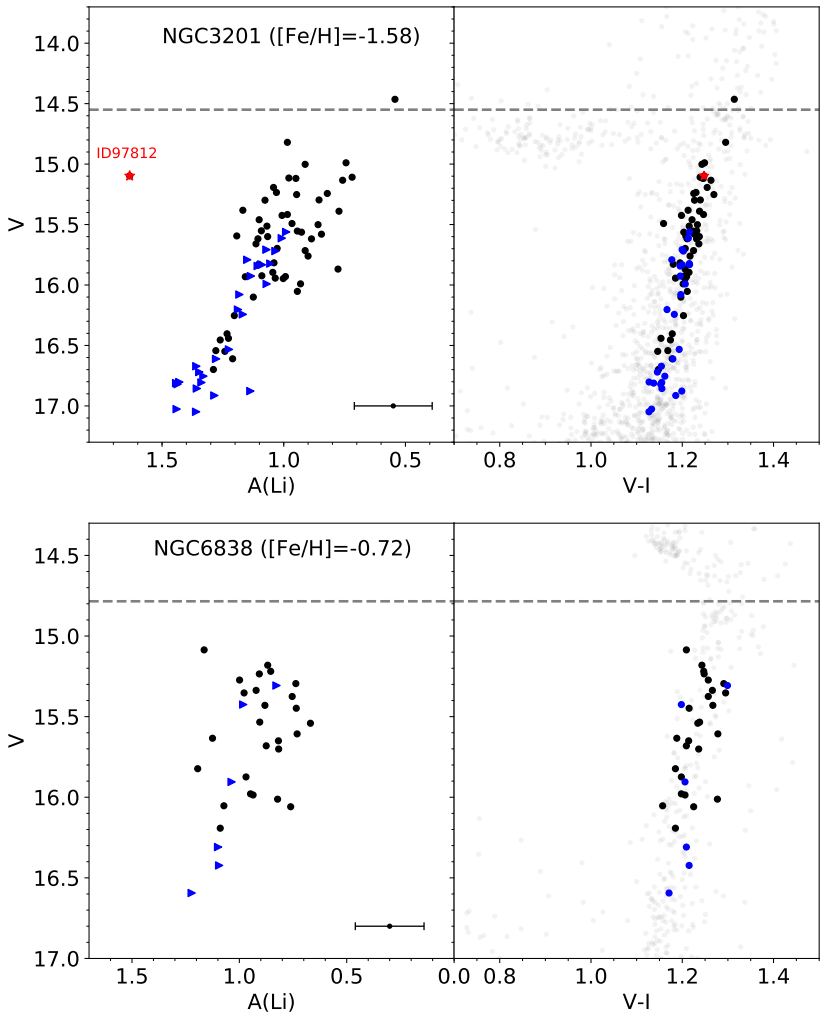

Fig. 3. Lithium abundances in NGC 3201 (*top panels*) and NGC 6838 (*bottom panels*) as a function of V magnitude (*left panels*), with their respective color-magnitude diagrams (*right panels*). Blue symbols are Li upper limits. The Li-rich red giant ID 97812 is marked as a red star. The dashed lines shows the position of the luminosity function bump.

not have a constant value is in NGC 3201. Here, we observe a decrease in the abundance from higher to lower temperatures. The presence of a plateau is much harder to identify and its value depends slightly on the position of the bins. If we define the plateau considering the three bins between ~4900 K to ~5050 K, where the abundance seems to be constant, we find a mean abundance of $A(\mathrm{Li}) = 0.97 \pm 0.10$ dex. Changing the bin size and position of bins, the mean A(Li) varies from 0.93 to 0.98 dex, with a similar standard deviation. The main difference between this and other clusters in our sample is its age, but there is no clear explanation to the larger scatter near the plateau. The scatter is fully consistent with the total error, which includes both the uncertainties due to quality of the spectra and uncertainties due to stellar parameters, especially the effective temperature.

We used our Li abundances together with theoretical stellar evolutionary models to predict an initial Li value in these clusters. We used the Yale Rotating Evolutionary code (YREC, Pinsonneault et al. 1989; Demarque et al. 2008), without diffusion, rotation, or overshooting. The models use mixing length theory for convection (Cox & Giuli 1968), which acts as the only mixing mechanism inside the star, with no extra-mixing to modify the surface abundances after the RGB bump. Additionally, we used 2006 OPAL equation of state (Rogers & Nayfonov 2002), and cross-section for the proton capture by lithium from Lamia et al. (2012). Other input physics included in these standard models can be found in Aguilera-Gómez et al. (2016). For each of the clusters, we ran models with a mass of $M = 0.8\,M_{\odot}$, considered to be the typical turn-off mass in globular clusters and a metallicity equal to the median value of the cluster (presented in Sect. 3).

The effects of diffusion, which can significantly change the lithium abundance in the main sequence evolutionary phase (Richard et al. 2002) are almost completely erased in the LRGB given that the diffusion layers are mixed again by the deepening convective envelope. The lithium abundance in the LRGB of standard models is at most 0.07 dex higher than when models include diffusion (Mucciarelli et al. 2012).

Models with an initial lithium abundance equal to the standard BBN value of $A(\mathrm{Li}) = 2.72$ dex produce LRGB Li values much larger than those observed. Instead, we attempt to find this primordial Li abundance. We modified the initial Li abundance of the models to match the Li in LRGB, post FDU dilution. These results can be seen in Fig. 6. The model presented for the cluster NGC 4590 has a metallicity of [Fe/H] ~ −2.2, which is the lowest metallicity we had available for the models. We tested that at such low metallicity, the initial abundance should not change significantly between that metallicity and the metallicity measured for the cluster ([Fe/H] = −2.34 dex).

Signatures of diffusion have been found in some globular clusters (e.g., Korn et al. 2006; Gruyters et al. 2016). The overall effect of diffusion in main sequence stars is to lower the surface Li abundance when approaching the turn-off; however,

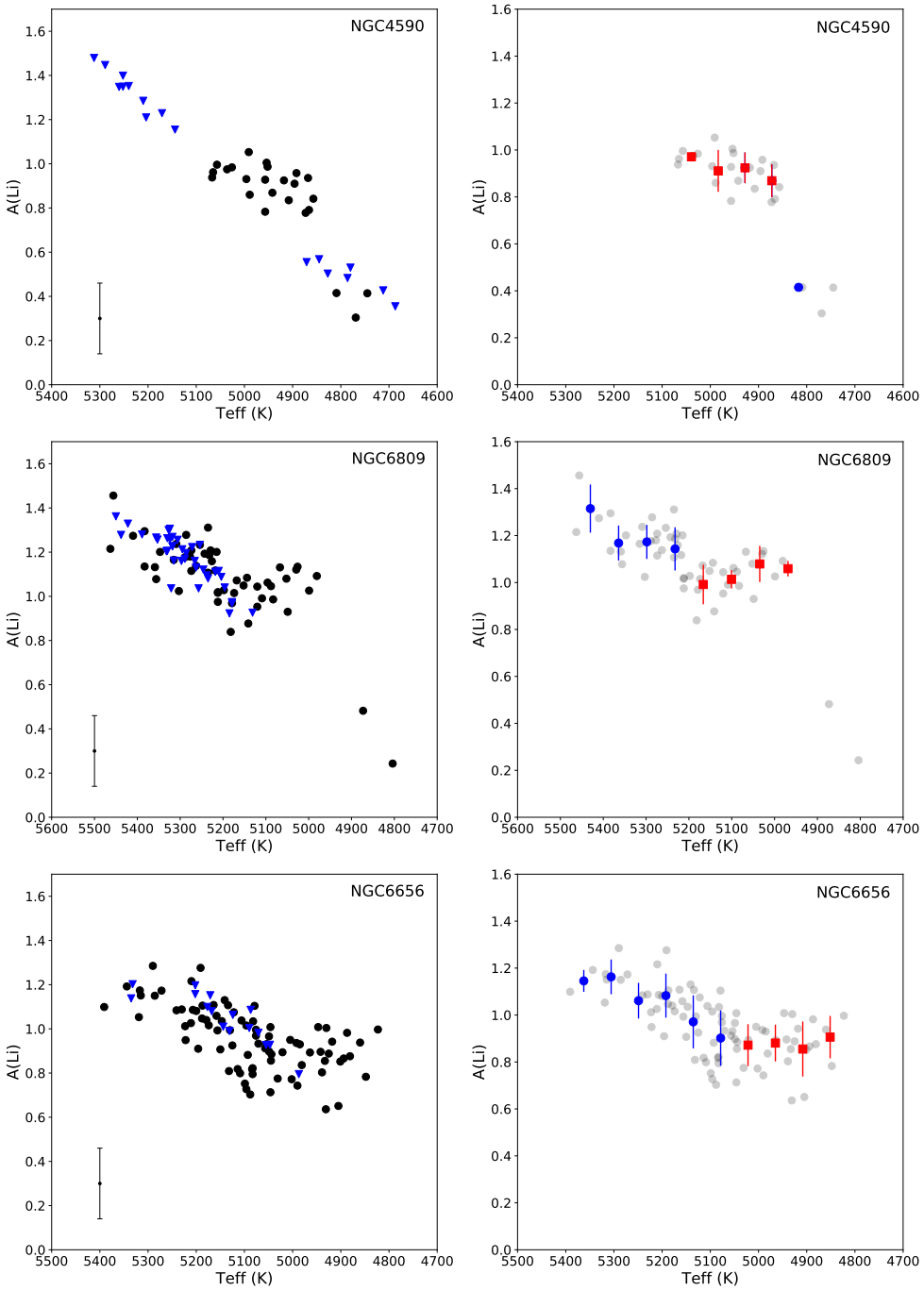

Fig. 4. Behavior of lithium abundances as a function of effective temperatures for NGC 4590, NGC 6809, and NGC 6656, *from top to bottom panels*. *Left panels*: abundances (black points) and upper limits (blue arrows). *Right panels*: measurements in gray and the binned Li abundances, considering equal-sized bins (blue points). Red squares mark the bins considered to be part of the Li LRGB plateau and used to calculate mean values reported.

observations suggest that the efficiency of diffusion is moderated by some competing mixing mechanism of unspecified origins. This makes it difficult to theoretically predict the Li abundance in the turn-off stars of our studied clusters using the measured LRGB as starting point. Thus, we did not attempt to predict a turn-off abundance and, instead, we recovered the initial, primordial Li abundances of these clusters with our models, considering that the effects of diffusion are erased during the FDU.

Predicted initial values in every case are very similar to the Spite plateau and A(Li) found in other globular clusters where the Li abundance can be measured in dwarfs. The inclusion of diffusion could decrease this predicted value by 0.07 dex at most. The primordial Li abundance of NGC 6809 is predicted to be $A(\mathrm{Li})_0 = 2.28$. We also included a model with 0.7 $M_\odot$ to see the effects that mass can have in the abundance of dwarfs in the cluster. In particular, Li burning, including in the pre-main sequence, can be substantially different in this mass range. By changing the mass of the model, and adjusting the Li in the LRGB, the predicted initial lithium changes by 0.08 dex, with a primordial value of $A(\mathrm{Li})_0 = 2.20$, both within values found in halo stars. The initial lithium predictions of the other clusters are $A(\mathrm{Li})_0 = 2.16$ in NGC 4590, $A(\mathrm{Li})_0 = 2.14$ for NGC 6656, $A(\mathrm{Li})_0 = 2.21$ in NGC 3201, and $A(\mathrm{Li})_0 = 2.17$ in NGC 6838. These predicted primordial A(Li) values calculated for each cluster match the Li abundances of the Spite plateau and other globular clusters in the literature.

We report in Table 4 LRGB stars abundances of the studied clusters and others in the literature. We also report in this table our predicted initial Li abundances and the Li abundance in the turn-off of clusters where it has been measured. We note here that

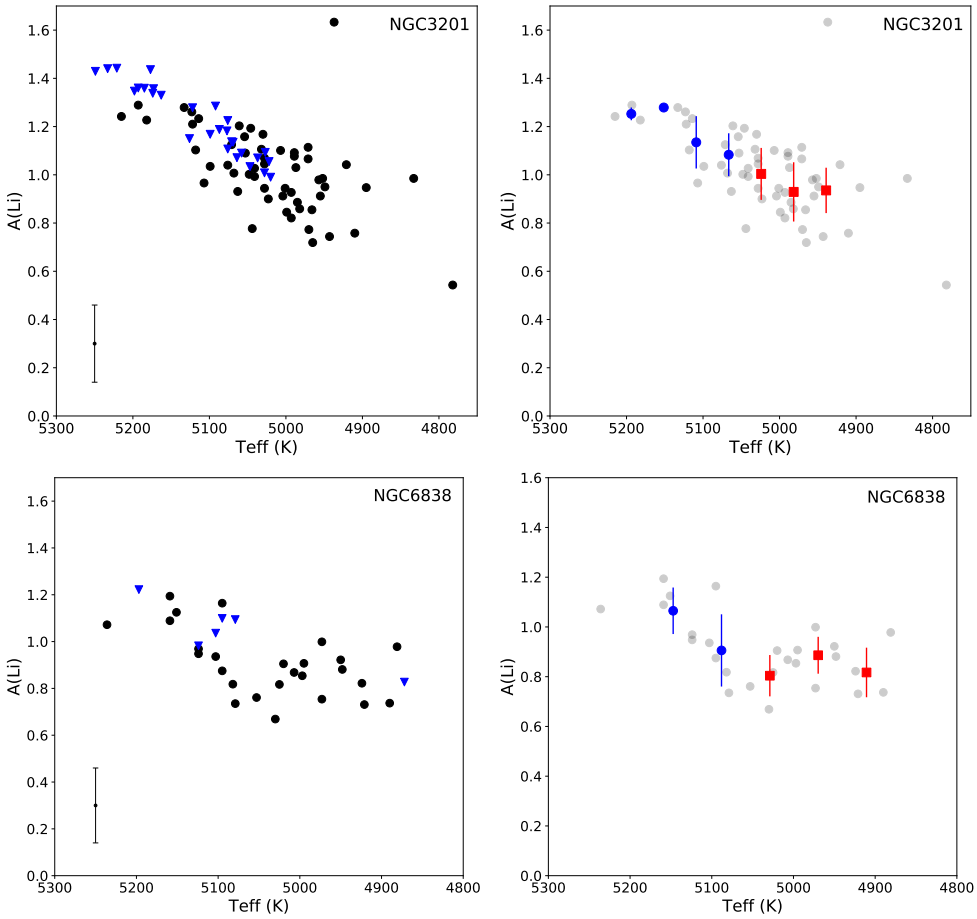

Fig. 5. Behavior of lithium abundances as a function of effective temperatures for NGC 3201 (*top panel*) and NGC 6838 (*bottom panel*). Same details as in Fig. 4.

the measurements are not homogeneous, and temperature scales can change the Li abundance measurements. There do not seem to be any correlations between the Li abundance in the LRGB (or the predicted primordial value) and metallicity for different clusters (Fig. 7).

The use of a different temperature scale could also change our Li measurements and estimated primordial abundances in the clusters. By using a hotter temperature scale (e.g., González Hernández & Bonifacio 2009), our Li abundances are expected to be higher by ~0.1 dex. The use of different stellar evolutionary models, or even different prescriptions in the model used (e.g., including overshooting or changing the efficiency of diffusion) can also modify the predicted estimation of cosmological Li (Mucciarelli et al. 2012), and even make it higher than the Spite plateau, although differences in the temperature scale of those measurements should also be taken into account (e.g., Meléndez & Ramírez 2004). Thus, our predictions should not be considered as an attempt to precisely obtain the exact primordial lithium of each cluster, but, rather, an estimation of the possible abundance range.

5.2. First and second population stars

Measurements of the Na abundance were made in order to separate populations in the studied globular clusters. This is based on the idea that the more massive stars of the first population, now evolved, had an active nucleosynthesis cycle in its interior able to produce, for instance, fresh Na at the expense of O. Throughout the lifetime of the star, this processed material is carried to the surface of the star, and through mass loss, stellar winds, and the planetary nebula phase, to the interstellar medium. The second population of stars is born from this polluted material, creating different populations of stars coexisting in the same cluster (see e.g., Bastian & Lardo 2018). The nature of the polluter is still a matter of open debate, with fast-rotating massive stars (Decressin et al. 2007) and asymptotic red giant branch stars (AGB, Ventura & D'Antona 2009) being the main contenders. On the other hand, there could be alternative scenarios to explain this pattern in clusters, not related to nucleosynthesis; or it is possible that the generational scenario is complicated by additional mechanisms that are at work (Gratton et al. 2019).

Li, which is destroyed at relatively low temperatures by proton capture, is expected to be depleted in Na-enriched material, from which second population stars are born. An anticorrelation between Na and Li is then expected. However, in certain AGB stars, Li can be created in the interior through the Cameron-Fowler mechanism (Cameron & Fowler 1971), and is quickly transported to the surface of the star by convection, where the cooler temperatures prevent it from destruction by proton capture (Sackmann & Boothroyd 1992). Thus, it may be relevant to compare the Li abundance from the first and second population, with the first population expected to have a cosmological Li content diluted because of the FDU, and the second population may show an abnormally high Li abundance if the polluter is either a Li-enriched AGB star or if the ejecta of polluters is mixed with material that has not burned Li.

Figures 8 and 9 show the behavior of A(Li) as a function of [Na/Fe] only for RGB stars in NGC 4590 and NGC 6809 (top and bottom panels of Fig. 8, respectively), and NGC 6656 and NGC 3201 (top and bottom panels of Fig. 9). We removed stars

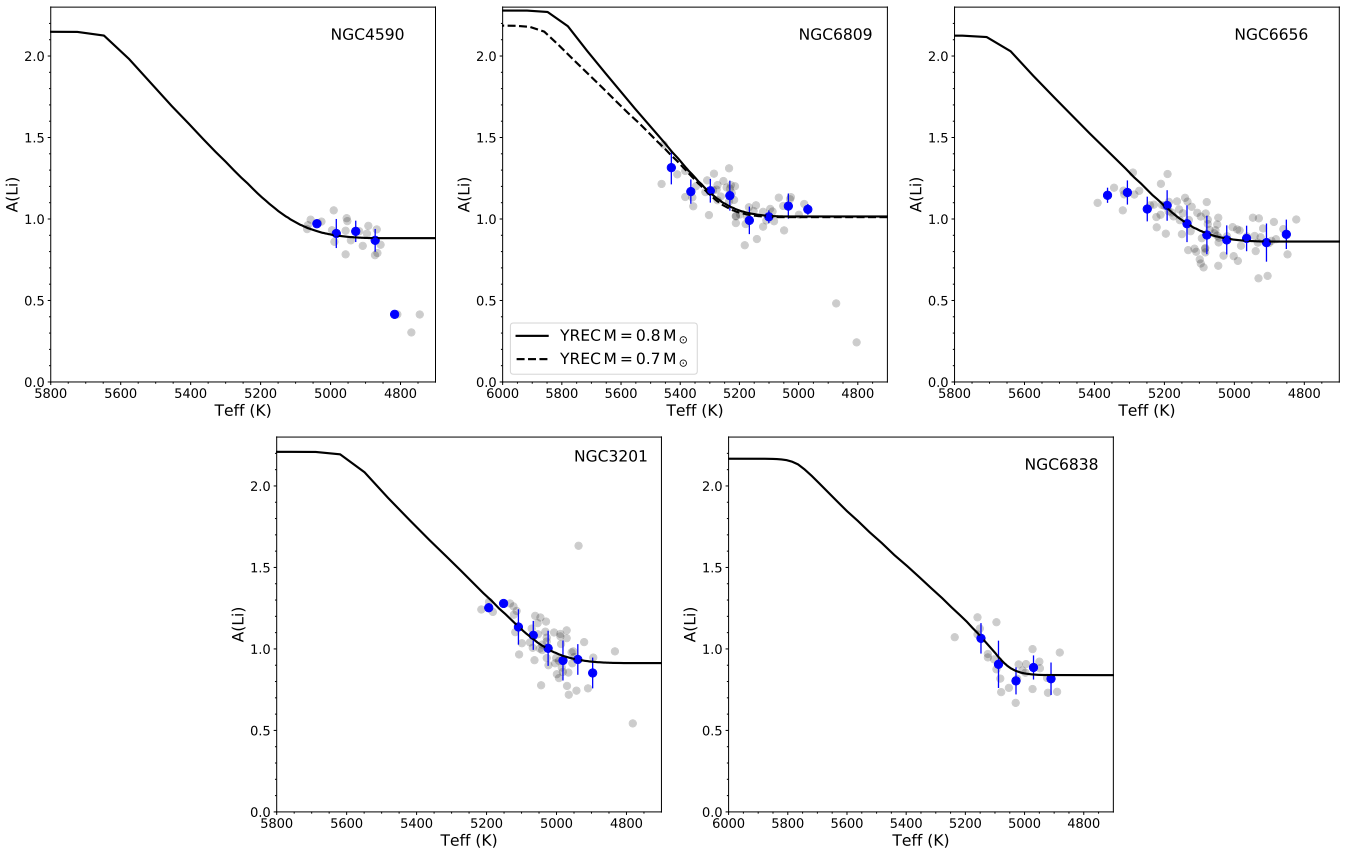

Fig. 6. Lithium abundance as a function of effective temperature. Blue points are the binned abundance in equal-sized bins. We include theoretical models that fit the LRGB Li plateau. In the cluster NGC 6809, we include models with 0.7 and 0.8 $M_{\odot}$.

Table 4. Lithium abundance in the LRGB plateau and turn-off of galactic globular clusters.

Cluster	[Fe/H]	$A(\mathrm{Li})_{\mathrm{LRGB}}$	$A(\mathrm{Li})_0$	Reference
–	(dex)	(dex)	(dex)	–
NGC 4590	−2.34	0.90 ± 0.08	2.16	This work
NGC 6809	−1.79	1.03 ± 0.08	2.28	This work
NGC 6656	−1.77	0.88 ± 0.09	2.14	This work
NGC 3201	−1.58	0.97 ± 0.10	2.21	This work
NGC 6838	−0.72	0.84 ± 0.10	2.17	This work
Cluster	[Fe/H]	$A(\mathrm{Li})_{\mathrm{LRGB}}$	$A(\mathrm{Li})_{\mathrm{TO}}$	Reference
NGC 7099	−2.30	1.10 ± 0.06	2.21 ± 0.12	1 [(a)]
NGC 6397	−2.10	1.13 ± 0.09	2.25 ± 0.01 ± 0.09	2 [(a)]
M4	−1.10	0.92 ± 0.01 ± 0.08	2.30 ± 0.02 ± 0.10	3 [(a)]
M4	−1.31	–	2.13 ± 0.09	4
NGC 6752	−1.68	0.83 ± 0.15	–	5
NGC 1904	−1.60	0.97 ± 0.02 ± 0.11	–	6
NGC 2808	−1.14	1.06 ± 0.02 ± 0.13	–	6
NGC 362	−1.26	1.02 ± 0.01 ± 0.11	–	6
NGC 6218	−1.37	1.07 ± 0.01 ± 0.06	–	7
NGC 5904	−1.29	1.02 ± 0.01 ± 0.11	–	7
47 Tuc	−0.76	–	1.78 ± 0.18	8
M92	−2.00	–	2.36 ± 0.19	9
ω Cen	−1.50	–	2.19 ± 0.14	10

Notes. [(a)]These works present Li abundances in the turn-off and lower red giant branch.
References. (1) Gruyters et al. (2016); (2) Lind et al. (2009b); (3) Mucciarelli et al. (2011); (4) Monaco et al. (2012); (5) Mucciarelli et al. (2012); (6) D'Orazi et al. (2015b); (7) D'Orazi et al. (2014); (8) Dobrovolskas et al. (2014); (9) Bonifacio (2002); (10) Monaco et al. (2010).

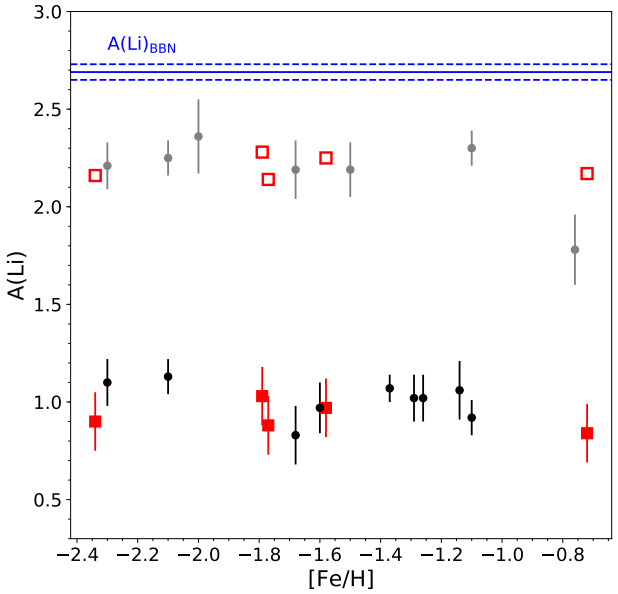

Fig. 7. Li abundance in the LRGB of the five studied globular clusters as a function of [Fe/H] (filled red squares). The calculated primordial abundances for these clusters are the empty red squares. These are compared to literature measurements of the lithium abundance in the LRGB (black points at low Li abundances) and in the turn-off stars (grey points at high Li abundances) of globular clusters in the Galaxy. Also, the Big Bang nucleosynthesis prediction from Coc et al. (2014) is included and shown as a blue line, with the dashed blue lines representing its reported uncertainties.

brighter than the RGB bump in these figures. Additionally, we considered only LRGB plateau stars in the right panel of these figures, by removing all stars that have not yet completed their first dredge-up. As mentioned in Sect. 4, we were not able to measure Na in NGC 6838; thus, we do not present results for that cluster. Focusing only on LRGB stars, there is no clear correlation between Li and Na in NGC 4590, NGC 6809, NGC 3201, and NGC 6656. We do see some star-to-star scatter, but Li does not scale with Na. This, however, does not exclude the possibility of finding a trend if more stars were to be considered in the analysis.

As previously mentioned, there is no statistically significant anticorrelation in NGC 6656. By eye, when considering all RGB stars of different effective temperatures in the top left panel of Fig. 9, objects with higher Na would seem to have slightly lower Li. However, when we look for possible correlations by binning both in effective temperature and Na, only the higher temperature bin shows a hint of an anticorrelation; however it is not considered statistically significant.

The lack of a clear Li-Na anticorrelation in our cluster sample requires further confirmation with additional data. In the literature, some clusters do show correlations between Li and other light element abundances. NGC 6752 presents a Li-O correlation (Shen et al. 2010) and Li-Na anticorrelation (Pasquini et al. 2005). NGC 6397 has some stars enriched in Na that are Li poor (Lind et al. 2009b). NGC 2808 has some stars enriched in Al that are Li depleted (D'Orazi et al. 2015b). In M4, there is something like a Li-Na anticorrelation (Monaco et al. 2012) but no Li-O correlation (Mucciarelli et al. 2011); 47 Tuc shows no sign of a Li-Na anticorrelation (Dobrovolskas et al. 2014).

If it is confirmed that some clusters have a similar Li abundance in both populations, this would point to a higher Li than expected in the second population. This could mean that the birth material of these stars should have been mixed with relatively Li-rich material, pointing to AGB stars as possible polluters. Models have to be fine-tuned to produce such a pattern in globular clusters, given that the Li yields have great uncertainties depending on how physics such as mass loss is introduced (Ventura & D'Antona 2010). If massive stars were the polluter, this scenario would require mixing the Na-rich material from the ejecta with unprocessed material that has a higher Li abundance. However, confirmation of the lack of a Na-Li anticorrelation is needed before anything can be firmly concluded about the mechanism behind the different populations in clusters. Additionally, measurements from clusters come from non-homogeneous sources that not only have different parameters scales and spectral qualities, and they use different methods, but these sources also provide the abundances for different light elements. An homogeneous determination of properties and abundances could be a major contribution in improving our knowledge of second generation polluters.

5.3. Li-rich giant in NGC 3201

Stars on the red giant branch experience abundance changes during the FDU, and then, at the luminosity function bump where the extra-mixing acts. If a solar-like star enters the RGB phase with a meteoritic abundance $A(\mathrm{Li}) = 3.3$, its predicted Li abundance after the FDU is expected to be $A(\mathrm{Li}) = 1.5$, only considering FDU dilution. However, the values can be much lower when additional ingredients, such as a much lower initial Li abundance, Li burning, and main-sequence mixing are taken into account. The precise value to classify a giant as enriched is actually mass- and metallicity-dependent, and standard giants with higher A(Li) than 1.5 dex can be found, as well as giants with lower abundances that could have experienced a Li-enrichment process (Aguilera-Gómez et al. 2016). In spite of predictions from canonical models, lithium-rich red giants, with higher Li abundances, even reaching or exceeding the meteoritic value, are known to exist (e.g., Wallerstein & Sneden 1982; Monaco et al. 2011).

Globular clusters present an advantage, with all of their giants sharing a similar mass, and possibly, a similar original Li content. Because of this, we can compare the Li abundance of the giants to abundances of other stars with similar parameters and at a similar evolutionary stage, making enriched objects much easier to identify. Although Li-rich giants are unusual in general, they are particularly rare in globular clusters. Only about a dozen giants are known to have a much higher Li abundance than other stars in the same evolutionary stage in a globular cluster. So far, Li enriched RGB stars have been found in NGC 5272 (Kraft et al. 1999), NGC 362 (Smith et al. 1999; D'Orazi et al. 2015a), NGC 4590 (Ruchti et al. 2011; Kirby et al. 2016), NGC 5053, NGC 5897 (Kirby et al. 2016), 2 giants in NGC 7099 (Kirby et al. 2016), ω Cen (Mucciarelli et al. 2019), and only one Li-rich star in NGC 1261 (Sanna et al. 2020).

These are located all along the RGB phase, although AGB Li-rich stars have also been found (e.g., Kirby et al. 2016). Some are located after the luminosity function bump of their respective clusters, where extra-mixing is expected to affect the abundance of stars and could be the reason behind the Li-enrichment. Before that point in evolution, other explanations must be invoked that require pollution from an external source or the presence of a binary companion to trigger Li production (Casey et al. 2019). In the case of pollution, the source could be an AGB companion that can produce additional lithium in its

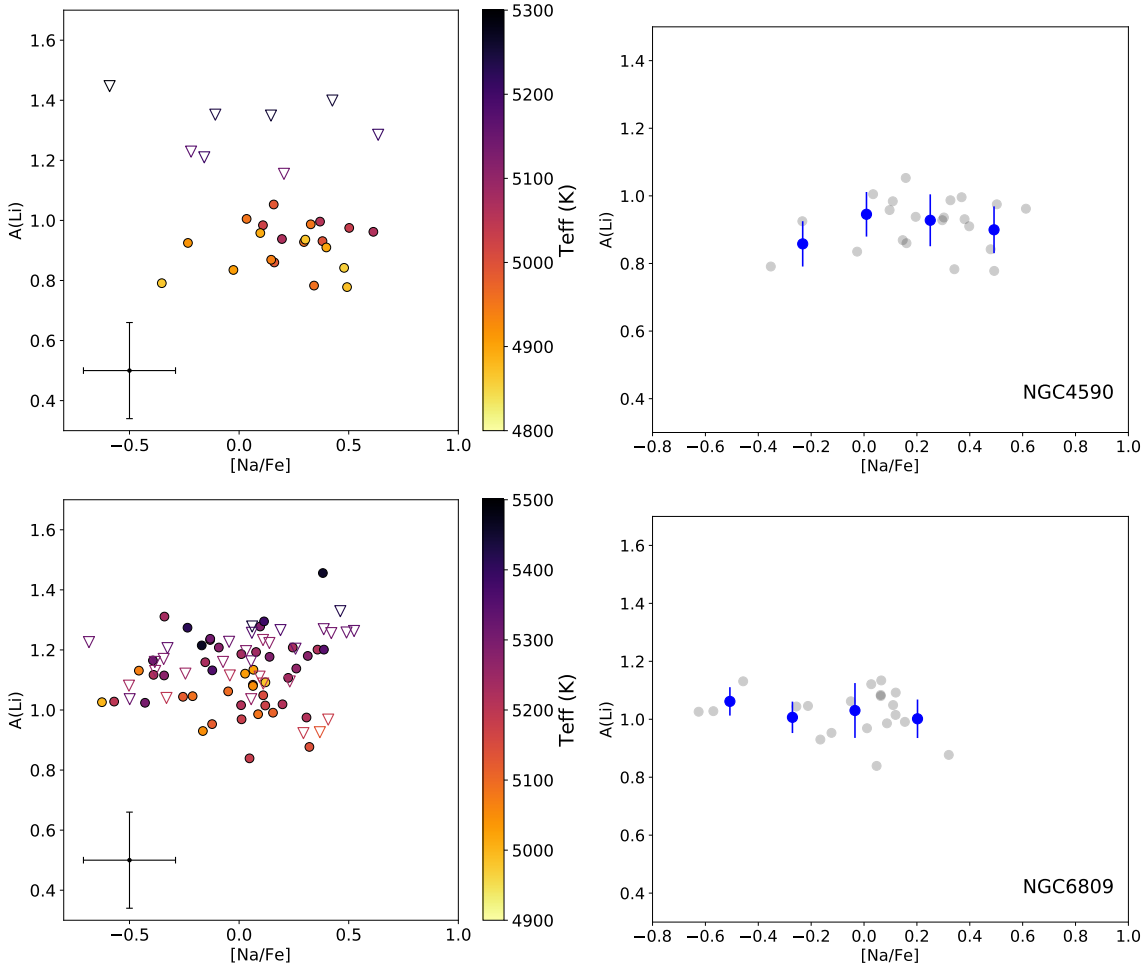

Fig. 8. Lithium abundance as a function of sodium abundance. *Left panel*: color-coded by effective temperature, and includes all RGB stars before the luminosity function bump, while the *right panel* considers only Li measurements (no upper-limits) of plateau LRGB stars, and it is binned (blue points) to show possible trends between both abundances. *Top panel*: NGC 4590, *bottom panel* shows NGC 6809.

interior and could then be transferring mass to the RGB star; it could be a nova that can produce Li during the thermonuclear runaway (Starrfield et al. 1978; Izzo et al. 2015); or a planet or brown dwarf accreted by the star, objects that preserve the Li they have at formation (Alexander 1967; Siess & Livio 1999).

We present the discovery here of one more Li-rich giant in a globular cluster, in this case, NGC 3201. The star ID 97812, with $A(\mathrm{Li})_{\mathrm{NLTE}} = 1.63 \pm 0.18$ dex is located before the luminosity function bump and thus it is not expected to be enriched by the internal production of Li. Instead, pollution, either during the RGB phase or before, is probably the cause of enrichment for this giant, it is still possible that the presence of a binary companion is triggering the Li enhancement. Considering accretion as a possible scenario, we calculate the Li abundance of the star after the engulfment of a planet, using the models and parameters from Aguilera-Gómez et al. (2016). Applying the Li abundance of the rest of stars in the cluster as the initial conditions for the model, we calculate the engulfed mass of a hypothetical planet needed to explain the high A(Li) of this star. This model is shown in Fig. 10. For Jupiter-like composition, a mass of $M_{\mathrm{planet}} = 10.1\, M_{\mathrm{Jupiter}} = 1.92 \times 10^{31}$ g is needed, and if the engulfed object had an Earth-like composition, it would require a mass of $M_{\mathrm{planet}} = 120\, M_{\mathrm{Earth}} = 7.17 \times 10^{29}$ g. Although the amount of Earth masses needed is high, the mass of the Jupiter-like planet required is in range of masses of exoplanets known that can orbit close to their parent star. Monitoring the radial velocity of this star would be interesting to understand if its enhancement comes from planet engulfment, or if a binary companion is responsible for its high Li abundance.

6. Summary

We calculated stellar parameters and measured Li and Na abundances of LRGB stars of five Galactic globular clusters, covering a wide range of metallicities from [Fe/H] = −0.72 to [Fe/H] = −2.34 dex. We find a LRGB plateau in all of the clusters at different levels, all between A(Li) = 0.84−1.03 dex, consistent with what has been found for other globular clusters previously.

Using theoretical models, we calculate the initial, primordial Li abundance in these clusters. The abundances found are similar to the Spite plateau value of halo stars, with A(Li) = 2.14−2.28. However, we note that the exact predicted value could change by using either a different temperature scale or different model. Thus, we use these predictions to conclude about the overall trends in Li abundances and not the exact value of the cosmological Li. As a caveat, we have to consider the possibility that the additional mixing operating during the main sequence which affects the efficiency of diffusion, might cause the transport of some extra Li in the burning regions (e.g., Richard et al. 2005).

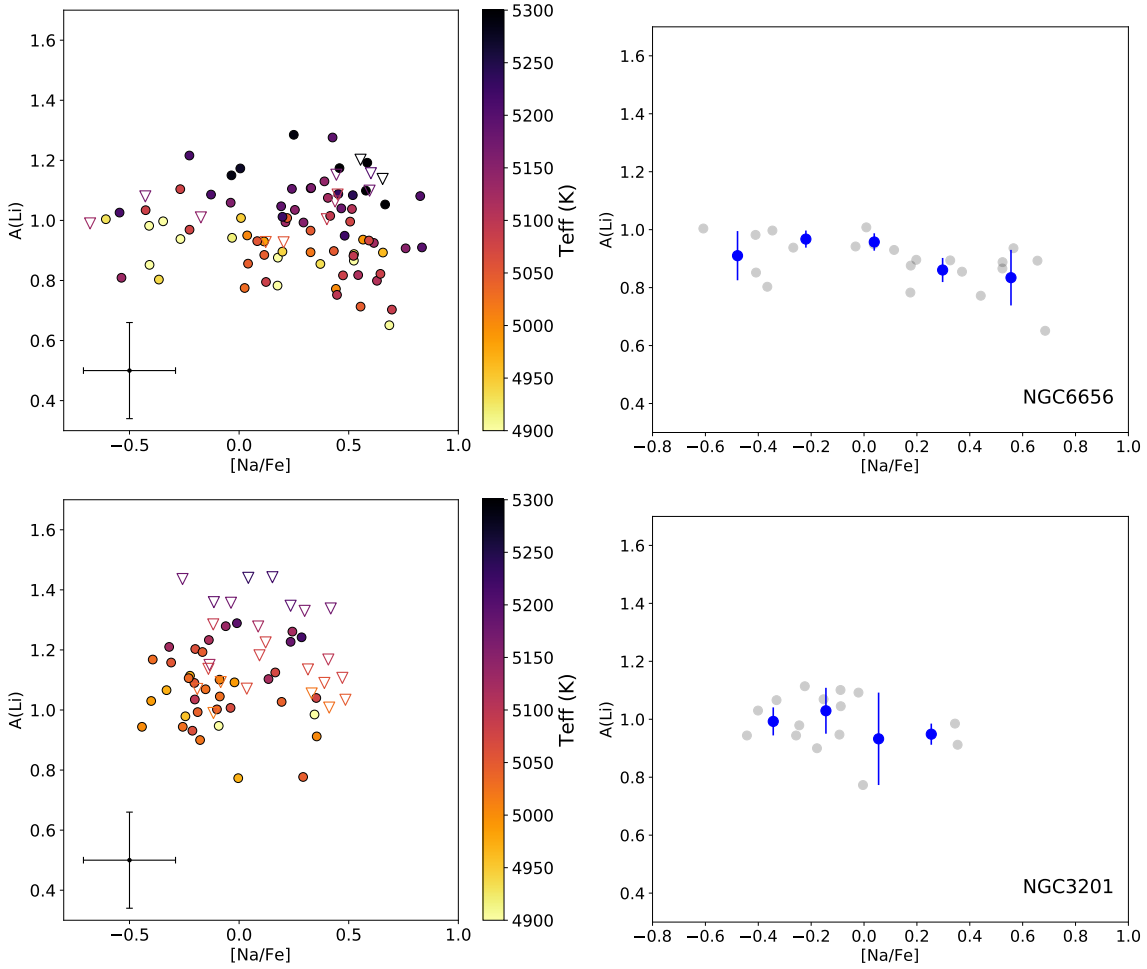

Fig. 9. Lithium abundance as a function of sodium abundance. Same details as in Fig. 8. *Top panels* are NGC 6656 and *bottom panels* are NGC 3201.

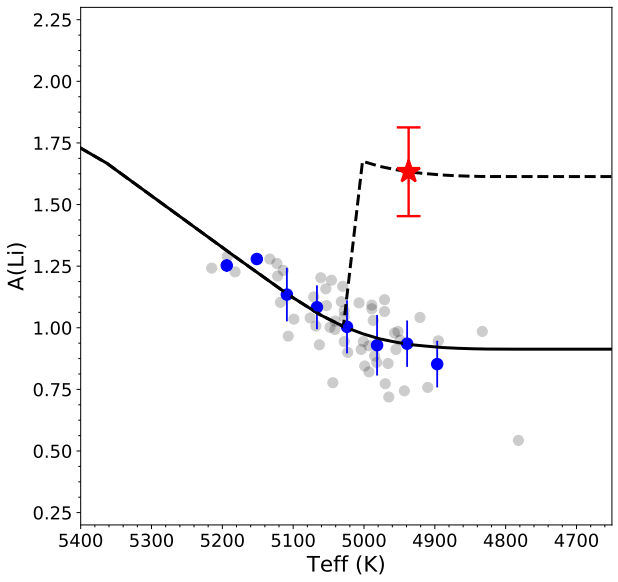

Fig. 10. Lithium abundance pattern of NGC 3201. The Li-rich giant found (red star) could be explained by a model with planet engulfment (dashed line), where the hypothetical planet has a mass of $M_{\rm planet}$ = 9.3 $M_{\rm Jupiter}$ (with Jupiter-like composition) or $M_{\rm planet}$ = 110 $M_{\rm Earth}$ with Earth-like composition.

This would result in an underestimate of the initial A(Li) from measurements of LRGB using standard stellar models.

Considering the uncertainties in Li abundances, our main conclusion is that all of the clusters are consistent with models that have evolved from the same initial Li abundance. This agrees with the idea of a constant Li abundance of stars at this metallicity range, confirming the large discrepancy between Big Bang nucleosynthesis predictions and observations of main sequence field stars.

We find no correlation between the Li value in the LRGB plateau and metallicity. To further study a possible correlation, we also use literature data available for other clusters, finding no relation between A(Li) and [Fe/H].

The measured sodium abundance is used to distinguish between first and second populations in each cluster. We find no clear difference in Li abundance between Na-rich and Na-poor stars in any of the clusters. If this is confirmed, it could point towards a class of polluter stars that are able to produce Li, such as AGB stars, or the mixing of the processed Li-poor medium with additional unprocessed matter. We summarize the main results for each of the studied clusters:

– NGC 4590: The median Li of LRGB stars in this metal-poor cluster is A(Li) = 0.90 ± 0.08 dex. Considering its metallicity of [Fe/H] = −2.34 ± 0.10 dex, we calculate an initial Li abundance $A(\mathrm{Li})_0$ = 2.16. There is no clear correlation between Na and Li in this cluster when we only consider LRGB stars.

- NGC 6809: The distribution of LRGB Li abundances in the cluster presents a peak at $A(\mathrm{Li}) = 1.03 \pm 0.08$ dex. The primordial value predicted, considering a RGB mass of $0.8\,M_{\odot}$ is $A(\mathrm{Li})_0 = 2.28$. This is the cluster with the highest Li abundances in the LRGB plateau in our sample. It does not present a Li-Na correlation either.
- NGC 6656: In this cluster, the LRGB plateau is located at $A(\mathrm{Li}) = 0.88 \pm 0.09$ dex, with a predicted initial value of $A(\mathrm{Li})_0 = 2.14$.
- NGC 3201: The RGB Li plateau is harder to identify in the cluster, as there appears to always be a small decrease in the abundance at decreasing temperatures. Considering this, we can define the LRGB stars between ~4900 K and ~5050 K and find a median abundance of $A(\mathrm{Li}) = 0.97 \pm 0.10$ dex. Calibrating models to that value we find an initial $A(\mathrm{Li})_0 = 2.21$. There is a Li-rich giant in this cluster with $A(\mathrm{Li}) = 1.63 \pm 0.18$ dex, located before the luminosity function bump. Its evolutionary state indicates that its high Li abundance might be the product of external pollution and, possibly, an accreted planet.
- NGC 6838: Although the number of stars in this cluster is small, we are able to find a Li plateau value of $A(\mathrm{Li}) = 0.84 \pm 0.10$ dex. This implies a primordial $A(\mathrm{Li})_0 = 2.17$. As it is the most metal-rich cluster in our sample, with $[\mathrm{Fe/H}] = -0.72 \pm 0.07$ dex, we can compare its abundances with 47 Tuc. The similar LRGB Li abundance of NGC 6838 with other clusters of lower metallicities suggests that if all higher metallicity globular clusters experience main sequence depletion similar to 47 Tuc, the effect is mostly erased when they evolve to the RGB phase. It is also possible that 47 Tuc is a peculiar case of main sequence depletion. More abundance measurements of clusters at this high metallicity are needed to understand if either NGC 6838 or 47 Tuc are unusual when compared to similar clusters.

Acknowledgements. We would like to thank the anonymous referee for their careful reading of the manuscript and helpful comments and suggestions. C.A.G. acknowledges support from the National Agency for Research and Development (ANID) FONDECYT Postdoctoral Fellowship 2018 Project number 3180668. This research was supported in part by the National Science Foundation under Grant No. PHY-1430152 (JINA Center for the Evolution of the Elements).

References

Aguado, D. S., González Hernández, J. I., Allende Prieto, C., & Rebolo, R. 2019, ApJ, 874, L21
Aguilera-Gómez, C., Chanamé, J., Pinsonneault, M. H., & Carlberg, J. K. 2016, ApJ, 829, 127
Albornoz, Á. L., Villanova, S., Cortés, C. C., Ahumada, J. A., & Parisi, C. 2021, AJ, 161, 76
Alexander, J. B. 1967, The Observatory, 87, 238
Alonso, A., Arribas, S., & Martínez-Roger, C. 1999, A&AS, 140, 261
Alonso-García, J., Mateo, M., Sen, B., et al. 2012, AJ, 143, 70
Aoki, M., Primas, F., Pasquini, L., et al. 2021, A&A, 653, A13
Bastian, N., & Lardo, C. 2018, ARA&A, 56, 83
Bergemann, M., Lind, K., Collet, R., Magic, Z., & Asplund, M. 2012, MNRAS, 427, 27
Bessell, M. S. 1983, PASP, 95, 480
Bonatto, C., Campos, F., & Kepler, S. O. 2013, MNRAS, 435, 263
Bonifacio, P. 2002, A&A, 395, 515
Bonifacio, P., Caffau, E., Spite, M., et al. 2018, A&A, 612, A65
Bruntt, H., Basu, S., Smalley, B., et al. 2012, MNRAS, 423, 122
Cameron, A. G. W., & Fowler, W. A. 1971, ApJ, 164, 111
Carretta, E., Bragaglia, A., Gratton, R., D'Orazi, V., & Lucatello, S. 2009a, A&A, 508, 695
Carretta, E., Bragaglia, A., Gratton, R., & Lucatello, S. 2009b, A&A, 505, 139
Carretta, E., Bragaglia, A., Gratton, R. G., et al. 2009c, A&A, 505, 117
Casey, A. R., Ho, A. Y. Q., Ness, M., et al. 2019, ApJ, 880, 125
Castelli, F., & Kurucz, R. L. 2003, in Modelling of Stellar Atmospheres, eds. N. Piskunov, W. W. Weiss, & D. F. Gray, 210, A20
Cayrel, R. 1988, in The Impact of Very High S/N Spectroscopy on Stellar Physics, eds. G. Cayrel de Strobel, & M. Spite, 132, 345
Chanamé, J., Pinsonneault, M., & Terndrup, D. M. 2005, ApJ, 631, 540
Charbonnel, C., & Primas, F. 2005, A&A, 442, 961
Choi, J., Dotter, A., Conroy, C., et al. 2016, ApJ, 823, 102
Coc, A., Uzan, J.-P., & Vangioni, E. 2014, JCAP, 2014, 050
Coelho, P., Barbuy, B., Meléndez, J., Schiavon, R. P., & Castilho, B. V. 2005, A&A, 443, 735
Cox, J. P., & Giuli, R. T. 1968, Principles of stellar structure
Da Costa, G. S., Held, E. V., Saviane, I., & Gullieuszik, M. 2009, ApJ, 705, 1481
De Angeli, F., Piotto, G., Cassisi, S., et al. 2005, AJ, 130, 116
Decressin, T., Meynet, G., Charbonnel, C., Prantzos, N., & Ekström, S. 2007, A&A, 464, 1029
Demarque, P., Guenther, D. B., Li, L. H., Mazumdar, A., & Straka, C. W. 2008, Ap&SS, 316, 31
Denissenkov, P. A., & VandenBerg, D. A. 2003, ApJ, 593, 509
Dobrovolskas, V., Kučinskas, A., Bonifacio, P., et al. 2014, A&A, 565, A121
D'Orazi, V., Lucatello, S., Gratton, R., et al. 2010, ApJ, 713, L1
D'Orazi, V., Angelou, G. C., Gratton, R. G., et al. 2014, ApJ, 791, 39
D'Orazi, V., Gratton, R. G., Angelou, G. C., et al. 2015a, ApJ, 801, L32
D'Orazi, V., Gratton, R. G., Angelou, G. C., et al. 2015b, MNRAS, 449, 4038
Dotter, A. 2016, ApJS, 222, 8
Ferraro, F. R., Messineo, M., Fusi Pecci, F., et al. 1999, AJ, 118, 1738
Fields, B. D. 2011, Annu. Rev. Nucl. Part. Sci., 61, 47
Fu, X., Bressan, A., Molaro, P., & Marigo, P. 2015, MNRAS, 452, 3256
Gaia Collaboration (Brown, A. G. A., et al.) 2018, A&A, 616, A1
González Hernández, J. I., & Bonifacio, P. 2009, A&A, 497, 497
González Hernández, J. I., Bonifacio, P., Caffau, E., et al. 2009, A&A, 505, L13
Gratton, R. G., Sneden, C., Carretta, E., & Bragaglia, A. 2000, A&A, 354, 169
Gratton, R., Bragaglia, A., Carretta, E., et al. 2019, A&ARv, 27, 8
Gray, R. O., & Corbally, C. J. 1994, AJ, 107, 742
Gruyters, P., Lind, K., Richard, O., et al. 2016, A&A, 589, A61
Harris, W. E. 1996, AJ, 112, 1487
Hinshaw, G., Larson, D., Komatsu, E., et al. 2013, ApJS, 208, 19
Izzo, L., Della Valle, M., Mason, E., et al. 2015, ApJ, 808, L14
Kains, N., Arellano Ferro, A., Figuera Jaimes, R., et al. 2015, A&A, 578, A128
Kayser, A., Hilker, M., Grebel, E. K., & Willemsen, P. G. 2008, A&A, 486, 437
Kirby, E. N., Guhathakurta, P., Zhang, A. J., et al. 2016, ApJ, 819, 135
Korn, A. J., Grundahl, F., Richard, O., et al. 2006, Nature, 442, 657
Kraft, R. P., Peterson, R. C., Guhathakurta, P., et al. 1999, ApJ, 518, L53
Lamia, L., Spitaleri, C., La Cognata, M., Palmerini, S., & Pizzone, R. G. 2012, A&A, 541, A158
Lee, Y. W., Joo, J. M., Sohn, Y. J., et al. 1999, Nature, 402, 55
Lind, K., Asplund, M., & Barklem, P. S. 2009a, A&A, 503, 541
Lind, K., Primas, F., Charbonnel, C., Grundahl, F., & Asplund, M. 2009b, A&A, 503, 545
Lind, K., Asplund, M., Barklem, P. S., & Belyaev, A. K. 2011, A&A, 528, A103
Marín-Franch, A., Aparicio, A., Piotto, G., et al. 2009, ApJ, 694, 1498
Mashonkina, L. I., Sitnova, T. N., & Pakhomov, Y. V. 2016, Astron. Lett., 42, 606
McCall, M. L. 2004, AJ, 128, 2144
Meléndez, J., & Ramírez, I. 2004, ApJ, 615, L33
Meléndez, J., Casagrande, L., Ramírez, I., Asplund, M., & Schuster, W. J. 2010, A&A, 515, L3
Molaro, P., Cescutti, G., & Fu, X. 2020, MNRAS, 496, 2902
Monaco, L., Bonifacio, P., Sbordone, L., Villanova, S., & Pancino, E. 2010, A&A, 519, L3
Monaco, L., Villanova, S., Moni Bidin, C., et al. 2011, A&A, 529, A90
Monaco, L., Villanova, S., Bonifacio, P., et al. 2012, A&A, 539, A157
Mucciarelli, A. 2013, ArXiv e-prints [arXiv:1311.1403]
Mucciarelli, A., & Bonifacio, P. 2020, A&A, 640, A87
Mucciarelli, A., Salaris, M., Lovisi, L., et al. 2011, MNRAS, 412, 81
Mucciarelli, A., Salaris, M., & Bonifacio, P. 2012, MNRAS, 419, 2195
Mucciarelli, A., Pancino, E., Lovisi, L., Ferraro, F. R., & Lapenna, E. 2013, ApJ, 766, 78
Mucciarelli, A., Salaris, M., Bonifacio, P., Monaco, L., & Villanova, S. 2014, MNRAS, 444, 1812
Mucciarelli, A., Lapenna, E., Massari, D., et al. 2015, ApJ, 809, 128
Mucciarelli, A., Salaris, M., Monaco, L., et al. 2018, A&A, 618, A134
Mucciarelli, A., Monaco, L., Bonifacio, P., et al. 2019, A&A, 623, A55
Pancino, E., Ferraro, F. R., Bellazzini, M., Piotto, G., & Zoccali, M. 2000, ApJ, 534, L83
Pasquini, L., Avila, G., Blecha, A., et al. 2002, The Messenger, 110, 1
Pasquini, L., Bonifacio, P., Molaro, P., et al. 2005, A&A, 441, 549
Pinsonneault, M. H., Kawaler, S. D., Sofia, S., & Demarque, P. 1989, ApJ, 338, 424

Planck Collaboration XVI. 2014, A&A, 571, A16
Prantzos, N. 2012, A&A, 542, A67
Richard, O., Michaud, G., & Richer, J. 2002, ApJ, 580, 1100
Richard, O., Michaud, G., & Richer, J. 2005, ApJ, 619, 538
Rogers, F. J., & Nayfonov, A. 2002, ApJ, 576, 1064
Ruchti, G. R., Fulbright, J. P., Wyse, R. F. G., et al. 2011, ApJ, 743, 107
Sackmann, I. J., & Boothroyd, A. I. 1992, ApJ, 392, L71
Samus, N., Kravtsov, V., Pavlov, M., Alcaino, G., & Liller, W. 1995, A&AS, 109, 487
Sanna, N., Franciosini, E., Pancino, E., et al. 2020, A&A, 639, L2
Sbordone, L., Bonifacio, P., Caffau, E., et al. 2010, A&A, 522, A26
Schlafly, E. F., & Finkbeiner, D. P. 2011, ApJ, 737, 103
Schlegel, D. J., Finkbeiner, D. P., & Davis, M. 1998, ApJ, 500, 525
Shen, Z. X., Bonifacio, P., Pasquini, L., & Zaggia, S. 2010, A&A, 524, L2
Siess, L., & Livio, M. 1999, MNRAS, 308, 1133
Simpson, J. D., Martell, S. L., Buder, S., et al. 2021, MNRAS, 507, 43
Smith, V. V., Shetrone, M. D., & Keane, M. J. 1999, ApJ, 516, L73
Sneden, C. A. 1973, PhD Thesis, The University of Texas at Austin
Spite, F., & Spite, M. 1982a, A&A, 115, 357
Spite, M., & Spite, F. 1982b, Nature, 297, 483
Starrfield, S., Truran, J. W., Sparks, W. M., & Arnould, M. 1978, ApJ, 222, 600
Stetson, P. B., & Pancino, E. 2008, PASP, 120, 1332
Stetson, P. B., Pancino, E., Zocchi, A., Sanna, N., & Monelli, M. 2019, MNRAS, 485, 3042
Tonry, J., & Davis, M. 1979, AJ, 84, 1511
VandenBerg, D. A., & Denissenkov, P. A. 2018, ApJ, 862, 72
Vasiliev, E., & Baumgardt, H. 2021, MNRAS, 505, 5978
Ventura, P., & D'Antona, F. 2009, A&A, 499, 835
Ventura, P., & D'Antona, F. 2010, MNRAS, 402, L72
Wallerstein, G., & Sneden, C. 1982, ApJ, 255, 577

Appendix A: Parameters and abundances

Table A.1. Measured atmospheric parameters and abundances for stars in the five globular clusters. Stetson IDs, V, and I magnitudes are from Stetson et al. (2019).

Gaia Source ID	Stetson ID	T_{eff} (K)	$\log g$ (dex)	v_t (km/s)	Flag A(Li)	$A(\mathrm{Li})_{\mathrm{NLTE}}$ (dex)	$[\mathrm{Na/Fe}]_{\mathrm{NLTE}}$	Vmag	Imag	SNR
3496356167836934016	67010	4780	1.68	1.67	<	0.53	-0.28	14.832	13.775	260.4
3496368228105102720	43508	4809	1.72	1.66		0.41	0.46	14.851	13.807	267.7
3496369254600313728	26784	4493	1.02	1.92	<	0.05	-0.02	13.7	12.501	439.5
3496369877372570752	41758	4866	1.87	1.62		0.79	-0.35	15.158	14.139	233.6
3496371183042641152	59548	4896	1.93	1.59		0.91	0.4	15.28	14.274	209.4
3496372931092316288	40799	4140	0.52	2.19	<	-0.65	-	12.673	11.252	760.1
3496366338319493504	24032	4827	1.6	1.7	<	0.5	-0.3	14.409	13.373	306.4
3496399422451210624	75588	4873	1.86	1.62		0.78	0.49	15.122	14.106	215.6
3496371079963753088	77334	4957	2.15	1.52		0.78	0.34	15.763	14.782	161.2
3496394616384561664	79098	4712	1.51	1.73	<	0.43	0.26	14.511	13.423	290.8
3496375684168708096	40678	4139	0.52	2.19	<	-0.67	-	12.717	11.295	783.7
3496375203132394112	69220	4942	2.1	1.54		0.87	0.15	15.66	14.673	184.2
3496371973316933888	70630	4892	1.95	1.59		0.96	0.1	15.344	14.336	197.9
3496372106461287936	73969	4845	1.71	1.66	<	0.57	-0.61	14.716	13.688	275.6
3496371664079202944	73337	4952	2.1	1.54		0.99	0.33	15.621	14.638	171.3
3496373244626964096	31721	4871	1.7	1.66	<	0.56	0.41	14.615	13.598	297.1
3496374687736171392	36851	4857	1.86	1.62		0.84	0.48	15.151	14.128	222.0
3496373210267235968	34954	4400	0.88	2.0		-0.52	-	13.348	12.097	567.1
3496374786518184960	36489	4954	2.07	1.55		1.0	0.03	15.527	14.545	185.2

Notes. Full table is available at the CDS.